Design and Experimental Demonstration of a Compact Silicon Photonic Interleaver Based on an Interfering Loop With Wide Spectral Range

Xinhong Jiang, Yuxing Yang, Hongxia Zhang, Jizong Peng, Yong Zhang, Ciyuan Qiu, and Yikai Su, *Senior Member, IEEE*

***Abstract*—We present the design and experimental demonstration of a compact tunable silicon photonic interleaver with a wide spectral range. The interleaver consists of an interfering loop containing a Fabry–Perot cavity formed by two Sagnac loops. The transmission coefficients of the directional couplers are calculated based on the maximally flat criterion. The impacts of the transmission coefficient variations on the extinction ratio and filter sharpness are investigated. The wavelength dependences of the directional couplers are analyzed to increase the spectral range of the interleaver. The device was fabricated on a silicon-on-insulator platform. The spectral ranges of the measured transmission and reflection spectra are increased to 60 nm. By thermal tuning the waveguide connecting the two Sagnac loops, the central wavelength can be shifted over one free spectral range with a wavelength-tuning efficiency of ∼0.08 nm/mW.**

***Index Terms*—Fabry–Perot, optical filters, sagnac interferometers, silicon photonics.**

I. Introduction

AN INTERLEAVER is a periodic optical filter that combines or separates dense wavelength division multiplexed (DWDM) signals [1]–[7]. Silicon photonic interleavers offer competitive advantages including compact footprint, low power consumption, and CMOS compatible fabrication [8], [9]. Various schemes have been proposed to realize silicon photonic interleavers [3], [9]–[12]. To obtain boxlike spectral responses, ring-assisted Mach-Zehnder interferometer (RA-MZI) structures [3], [10], [11] have been employed to improve the roll-off at the passband edges. However, the long cavity lengths of ring resonators are needed to achieve narrow channel spacing. In addition, the length difference of the two MZI arms should be half the ring circumference, which requires multiple phase shifters to tune the central wavelength. A ring-resonator MZI (RR-MZI) interleaver [9], [12] comprising a ring resonator and a directional coupler eliminates the length difference of the two arms. However, it still has a long cavity length to obtain narrow channel spacing. A silicon photonic interleaver using loop-mirror-based Michelson-Gires-Tournois interferometer (MGTI) was proposed in [13]. It takes advantage of the reflective optical paths to reduce the cavity length, but a precise control of length difference between the two arms is required [14], [15]. In our previous work [16], we proposed and experimentally demonstrated a compact silicon photonic interleaver using an interfering loop containing a Fabry-Perot (FP) cavity formed by two Sagnac loops to remove the length difference. Boxlike transmission spectrum in a ∼20-nm spectral range was measured at one output port. The reflection spectrum complementary to the transmission spectrum was not measured due to the high reflection power from the grating coupler to the input fiber.

In this paper, we perform a detailed study of design, fabrication, and characterization of the interleaver. To obtain flattop passbands, the transmission coefficients are calculated based on the maximally-flat criterion. Analysis reveals that the odd-order derivatives of the intensity transfer function vanish while the second-order derivative is dependent on the transmission coefficients. Therefore, by setting the second-order derivative to zero, the transmission coefficients can be obtained in a maximally-flat sense. The impacts of the transmission coefficient variations on the extinction ratio (ER) and filter sharpness are investigated. Then the wavelength dependences of the directional couplers are taken into consideration. By properly designing the directional couplers, high ERs can be obtained in the desired wavelengths, thus increasing the spectral range of the interleaver. In this paper, the spectral ranges of the measured transmission and reflection spectra are increased to 60 nm. The reflection spectrum is measured by inserting a directional coupler before the input of the interfering loop. The free spectral range (FSR) of the interleaver is ∼1.96 nm. By thermally tuning the waveguide connecting the two Sagnac loops, the central wavelength of the interleaver can be shifted over one FSR with a wavelength-tuning efficiency of ∼0.08 nm/mW.

The paper is organized as follows. Section II describes the device configuration and operation principle. The transmission coefficients of the directional couplers are calculated to realize flattop passbands. In Section III, the impacts of the transmission coefficient variations on the ER and filter sharpness are

Manuscript received March 1, 2017; revised April 25, 2017 and June 4, 2017; accepted June 19, 2017. Date of publication June 28, 2017; date of current version July 15, 2017. This work was supported in part by the National Natural Science Foundation of China under Grant 61235007/61505104/61605112, in part by the 863 High-Tech Program under Grant 2015AA017001, and in part by the Science and Technology Commission of Shanghai Municipality under Grant 15ZR1422800/16XD1401400. *(Corresponding author: Yikai Su.)*

The authors are with the State Key Laboratory of Advanced Optical Communication Systems and Networks, Department of Electronic Engineering, Shanghai Jiao Tong University, Shanghai 200240, China (e-mail: jiangxinhong@sjtu.edu.cn; sm_cat@sjtu.edu.cn; zhanghongxia@sjtu.edu.cn; pengjizong@sjtu.edu.cn; yongzhang@sjtu.edu.cn; qiuciyuan@sjtu.edu.cn; yikaisu@sjtu.edu.cn).

Color versions of one or more of the figures in this paper are available online at http://ieeexplore.ieee.org.

Digital Object Identifier 10.1109/JLT.2017.2720188

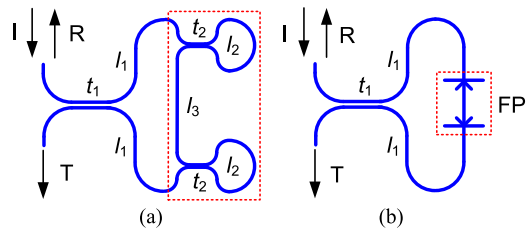

Fig. 1. (a) Schematic of the interleaver. (b) An equivalent structure. FP: Fabry-Perot.

investigated, and the wavelength dependences of the directional couplers are analyzed to increase the spectral range of the interleaver. Section IV presents the fabrication processes and experimental results of the device including measured transmission and reflection spectra, and central wavelength tuning. Finally, Section V provides the conclusion.

II. Device Configuration and Operation Principle

A. Device Configuration and Transmission Functions

The schematic of the interleaver is shown in Fig. 1(a). The device consists of a directional coupler and a FP cavity formed by two Sagnac loops. It is equivalent to the structure shown in Fig. 1(b). The light launched into the input port is split by the directional coupler. After passing and reflecting by the FP cavity, the lights are recombined and output through the directional coupler.

The transmission and reflection functions t_{T} and t_{R} of the interleaver can be written as:

$$t_T = a_1^2((t_1^2 - k_1^2)t_{\mathrm{FP}} + 2t_1k_1jr_{\mathrm{FP}}), \tag{1}$$

$$t_R = a_1^2((t_1^2 - k_1^2)r_{\mathrm{FP}} + 2t_1k_1jt_{\mathrm{FP}}), \tag{2}$$

$$t_{\mathrm{FP}} = (t_2^2 - k_2^2)^2a_2^2a_3/(1+4t_2^2k_2^2a_2^2a_3^2), \tag{3}$$

$$r_{\mathrm{FP}} = 2jt_2k_2(a_2 + a_2^3a_3^2)/(1+4t_2^2k_2^2a_2^2a_3^2), \tag{4}$$

where t_{FP} and r_{FP} are the transmission and reflection functions of the FP cavity, respectively. t_i and k_i ($t_i^2 + k_i^2 = 1$, $i = 1, 2$) are the transmission and coupling coefficients of the directional couplers, respectively. $a_i = \exp(-\alpha l_i - j\beta l_i)$ ($i = 1, 2, 3$) are the transmission factors of the waveguides, with l_i ($i = 1, 2, 3$) denoting the lengths of the waveguides. α is the loss factor and $\beta = 2\pi n_{\mathrm{g}}/\lambda$ is the propagation constant of the silicon waveguides. n_{g} is the group index. The cavity length of the FP cavity $L = l_2 + l_3$ determines the FSR ($= \lambda^2/(n_{\mathrm{g}}L)$), where l_2 and l_3 represent the lengths of a Sagnac loop and the waveguide connecting two Sagnac loops, respectively.

B. Theoretical Calculation of Transmission Coefficients

In the maximally-flat criterion, the derivatives of the intensity transfer function are used to describe the flatness of a filter [17]. Butterworth filters based on the maximally-flat criterion can be used to approximate the desired frequency responses [18]. Synthesis algorithms of Butterworth filters have been studied for various filter architectures such as rings, MZIs, and Bragg gratings [18], [19].

The derivatives of the intensity transfer function for our device are calculated to realize a maximally-flat response [20]. Since the intensity transfer function is an even function of the phase shift $\phi (= \beta L)$, the odd-order derivatives at $\phi = 0$ are zero. Therefore, by setting the second-order derivative to zero, the transmission coefficients can be obtained in a maximally-flat sense. In the following discussion, a lossless device ($\alpha = 0$) is considered. The group index n_g is 4.352 according to the fitting value from our previously fabricated devices. To achieve a FSR of $\sim$2 nm, the lengths of the waveguides are chosen as $l_1 = 41.89\,\mu$m, $l_2 = 64.83\,\mu$m, and $l_3 = 207.55\,\mu$m.

According to (1) and (2), the transmission and reflection functions t_{T} and t_{R} in z-domain can be expressed as:

$$H_T(z) = a_1^2a_2 \times \frac{-4t_1k_1t_2k_2 + (t_1^2 - k_1^2)(t_2^2 - k_2^2)^2z^{-1} - 4t_1k_1t_2k_2z^{-2}}{1 + 4t_2^2k_2^2z^{-2}}, \tag{5}$$

$$H_R(z) = 2ja_1^2a_2 \times \frac{(t_1^2 - k_1^2)t_2k_2 + t_1k_1(t_2^2 - k_2^2)^2z^{-1} + (t_1^2 - k_1^2)t_2k_2z^{-2}}{1 + 4t_2^2k_2^2z^{-2}}. \tag{6}$$

Here $z^{-1} = \exp(-j\phi) = \exp(-j\beta L)$ is half the round-trip delay of the FP cavity, ϕ is half the round-trip phase shift, and L is the cavity length. To obtain the same amplitudes in the passbands of $|H_{\mathrm{T}}(z)|$ and $|H_{\mathrm{R}}(z)|$, the condition $|H_{\mathrm{T}}(z)| = |H_{\mathrm{R}}(-z)|$ should be satisfied. As a result, $t_1^2 - k_1^2 = \pm 2t_1k_1$, $t_1 = 0.924$ or 0.383. Since the spectra of $|H_{\mathrm{T}}(z)|^2$ and $|H_{\mathrm{R}}(z)|^2$ are complementary, only $H_{\mathrm{T}}(z)$ needs to be studied. For simplicity, $H_{\mathrm{T}}(z)$ can be expressed as:

$$H_T(z) = a_1^2a_2\frac{a + bz^{-1} + az^{-2}}{1 + dz^{-2}},$$
$$a = -4t_1k_1t_2k_2,$$
$$b = (t_1^2 - k_1^2)(t_2^2 - k_2^2)^2,$$
$$d = 4t_2^2k_2^2. \tag{7}$$

Then $|H_{\mathrm{T}}(z)|^2$ is

$$|H_T(z)|^2 = \frac{(a + bz^{-1} + az^{-2})(a + bz + az^2)}{(1 + dz^{-2})(1 + dz^2)}. \tag{8}$$

At the center of the passbands, ϕ equals π and 0 for $t_1 = 0.924$ and 0.383, respectively. According to (5), the spectra of $|H_{\mathrm{T}}(z)|^2$ are complementary for $t_1 = 0.924$ and 0.383, thus it is sufficient to study the second-order derivative with $t_1 = 0.924$. The calculated $\mathrm{d}^2(|H_{\mathrm{T}}(z)|^2)/\mathrm{d}\phi^2$ at $\phi = \pi$ is

$$\mathrm{d}^2(|H_T(z)|^2)/\mathrm{d}\phi^2\Big|_{\phi=\pi} = \frac{8d(2a - b)^2}{(d+1)^4} + \frac{4ab - 8a^2}{(d+1)^2}. \tag{9}$$

Fig. 2(a) shows the absolute value of $\mathrm{d}^2(|H_{\mathrm{T}}(z)|^2)/\mathrm{d}\phi^2$ at $\phi = \pi$ as a function of t_2. The second-order derivatives are zero for $t_2 = 0.212$, 0.707, and 0.977. If $t_2 = 0.707$, the Sagnac loops act as total reflection mirrors, and the interleaver becomes a Michelson interferometer, thus it will not be used in the

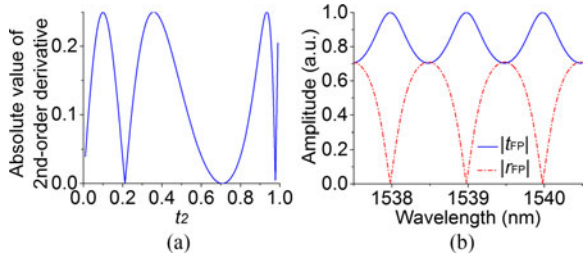

Fig. 2. (a) Absolute value of $\mathrm{d}^2(|H_{\mathrm{T}}(z)|^2)/\mathrm{d}\phi^2$ at $\phi = \pi$ as a function of t_2. (b) Transmission and reflection spectra of the FP cavity for $t_1 = 0.924$ and $t_2 = 0.977$.

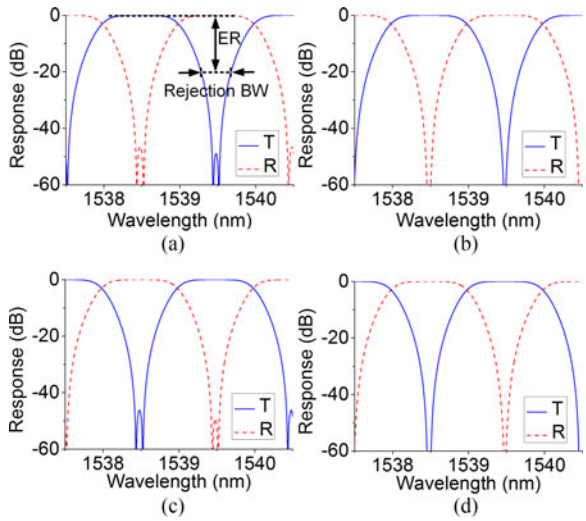

Fig. 3. Simulated transmission and reflection spectra with the four groups of (t_1, t_2): (a) (0.924, 0.977), (b) (0.924, 0.212), (c) (0.383, 0.977), and (d) (0.383, 0.212). BW: bandwidth. ER: extinction ratio.

following discussion. Since the derivatives are calculated in a small FSR of ~2 nm, the wavelength dependences of the directional couplers are not considered.

In the above analysis and calculations, four groups of (t_1, t_2) are obtained: (0.924, 0.977), (0.924, 0.212), (0.383, 0.977), and (0.383, 0.212). Fig. 3 shows the simulated transmission and reflection spectra with the four groups of transmission coefficients. As shown in Fig. 3(a) and (c), the transmission spectra for $t_1 = 0.924$ and 0.383 are complementary. The different ERs of the four groups are attributed to the finite precisions of the transmission coefficients in the simulations.

For a certain coupling gap, the transmission coefficient of a directional coupler decreases with the increase of the coupling length. To obtain a shorter coupling length with lower wavelength dependence, higher transmission coefficient is preferred [21]. Therefore, $t_1 = 0.924$ and $t_2 = 0.977$ will be used in the following discussion. The corresponding spectra of the FP cavity and the interleaver are shown in Figs. 2(b) and 3(a), respectively. Fig. 3(a) shows the rejection bandwidth corresponding to a certain ER [9]. The filter bandwidth can be defined as the smaller value of the 20-dB rejection bandwidth and the 1-dB passband width [18]. In Fig. 3(a), the FSR is ~2 nm. The 20-dB rejection bandwidth and the 1-dB passband width are 0.198 FSR and 0.395 FSR, respectively. Then the filter

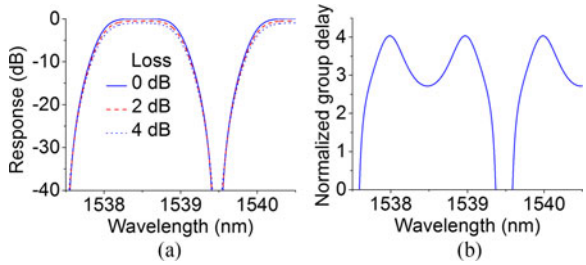

Fig. 4. (a) Transmission spectra at port T with different round-trip losses of the FP cavity. (b) Normalized group delay at port T for a round-trip loss of 1 dB.

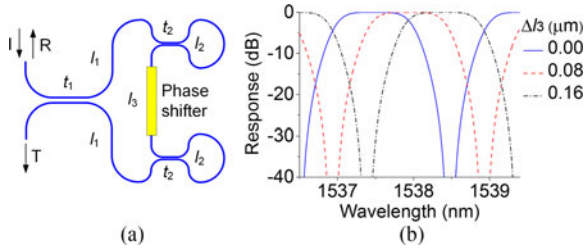

Fig. 5. (a) Tunable interleaver with one phase shifter. (b) Simulated wavelength tuning of the reflection spectrum.

bandwidth is 0.198 FSR. As a figure of merit of the roll-off sharpness [22], the shape factor is defined as the ratio of the 20-dB bandwidth to the 3-dB bandwidth [23]. The 3-dB and the 20-dB bandwidths are ~1 nm and ~1.6 nm, respectively, corresponding to a shape factor of ~1.6.

C. Impact of Waveguide Loss

Waveguide loss degrades the filter performance of the interleaver. Fig. 4(a) depicts the filter response as a function of the round-trip loss of the FP cavity. With increased waveguide loss, the filter sharpness decreases and the insertion loss increases.

D. Group Delay

Group delay is defined as [24], [25]:

$$\tau = -\frac{\partial \Phi}{\partial \omega} = -\frac{\partial \Phi}{\partial \theta} T = \tau_n T, \tag{10}$$

where Φ is the phase of the transmission function. ω is the angular frequency. $\theta = 2Ln_{\mathrm{g}} \times 2\pi/\lambda = 2Ln_{\mathrm{g}}\omega/c$ is the total phase shift for the light that runs one round in the FP cavity. c is the speed of light in vacuum. $T = 2Ln_{\mathrm{g}}/c$ is the unit delay of the FP cavity. τ_{n} is the normalized group delay. Fig. 4(b) presents the normalized group delays at port T for a round-trip loss of 1 dB. The maximum group delay is achieved at the resonance wavelengths of the FP cavity.

E. Simulation of Central Wavelength Tuning

The central wavelength of the interleaver can be shifted by tuning the phase shifter on the waveguide with a length of l_3, as shown in Fig. 5(a). The FSR of the FP cavity is half that of the interleaver. To obtain the same $\mathrm{FSR} = \lambda^2/(2Ln_{\mathrm{g}})$ as the FP cavity, the cavity length of a ring resonator should be $2L$. The resonance wavelengths of the FP cavity and the ring resonator are

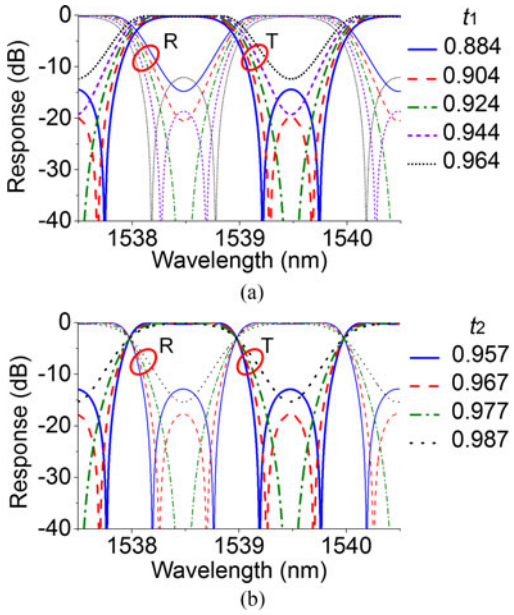

Fig. 6. Simulated transmission and reflection spectra for (a) various t_1 when $t_2 = 0.977$ and (b) various t_2 when $t_1 = 0.924$.

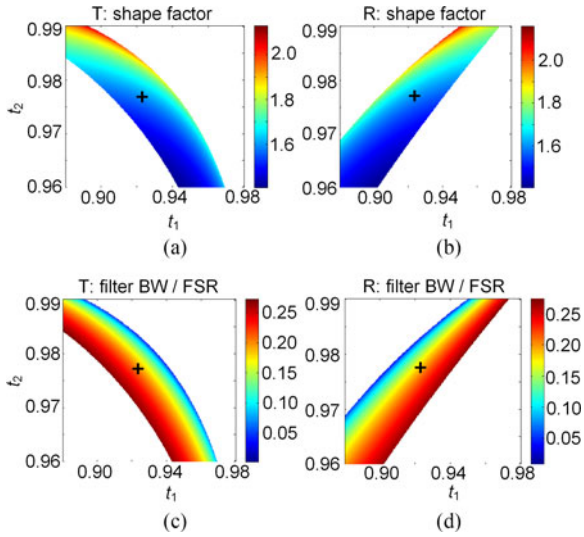

Fig. 7. (a)(b) The shape factors at ports (a) T and (b) R, respectively. (c)(d) The ratios of the filter bandwidths (BWs) to the FSR at ports (c) T and (d) R, respectively. The coordinate of the symbol '+' is (0.924, 0.977).

both $2Ln_g/N$ (N is an integer). With the same tuning power, the group index changes of the FP cavity and the ring resonator can be denoted as Δn_g and $\Delta n_g/2$, respectively. The corresponding resonance wavelength shifts are $\lambda\Delta n_g/n_g$ and $\lambda\Delta n_g/(2n_g)$, respectively. Therefore, the wavelength-tuning efficiency of the FP cavity is twice that of the ring resonator with the same FSR.

To tune the central wavelength, the phase shift $l_3 n_g$ of the waveguide is changed by increasing the group index n_g. For simplicity, the increase of n_g is equivalent to the increase of l_3 in the simulation. The central wavelength shift can be expressed as $\Delta\lambda = \lambda\Delta l_3/L$, where Δl_3 is the increase of l_3, and $L = l_2 + l_3$ is the cavity length of the FP cavity. The ratio of the central wavelength shift to the FSR change of the interleaver is $\Delta\lambda\,/\,\Delta\mathrm{FSR} = n_g\,(L + \Delta l_3)/\lambda$. For $L = 272.38\,\mu$m in our device, the central wavelength changes much more significantly than the FSR.

Fig. 5(b) presents the reflection spectra of wavelength tuning. The central wavelength tuning of the reflection spectrum is simulated by increasing l_3 to $l_3 + \Delta l_3$. The central wavelength is red-shifted by ~0.905 nm with Δl_3 changing from 0.00 μm to 0.16 μm.

III. Impacts of Transmission Coefficient Variations

To study the impacts of the transmission coefficient variations on the filter performance, the transmission and reflection spectra for different t_1 and t_2 are simulated. Assuming a lossless device, Fig. 6(a) shows the spectra with various t_1 when $t_2 = 0.977$. If t_1 is not 0.924, the ERs at ports T and R are not equal. When t_1 increases, the ERs first increase and then decrease at ports T and R. Meanwhile, the filter sharpness decreases at port T and increases at port R. Fig. 6(b) shows the spectra with various t_2 when $t_1 = 0.924$. For all t_2 values, the ERs at ports T and R are the same. With the increase of t_2, the ERs first increase and then decrease, and the filter sharpness decreases.

To further investigate the dependences of the filter sharpness on the transmission coefficients, the contour plots of the shape factors are provided in Fig. 7(a) and (b). The impacts of the transmission coefficient variations on the filter sharpness in Fig. 7(a) and (b) are consistent with that in Fig. 6. Fig. 7(c) and (d) show the contour plots of the ratios of the filter bandwidths to the FSR. The optimal transmission coefficients ($t_1 = 0.924$ and $t_2 = 0.977$) calculated in Section II(B) are indicated by the symbol '+' in the contour plots. The corresponding filter bandwidth is ~0.2 FSR and the shape factor is ~1.6 at ports T and R.

To achieve a wide spectral range, the wavelength dependences of the directional couplers need to be considered, which might degrade the filter performance at certain wavelengths. To obtain a filter response with high ERs in a wide spectral range, the optimal transmission coefficients should be designed at the central wavelength of the spectral range, thus the transmission coefficients in the spectral range do not deviate far from the optimal values.

IV. Experimental Results

Fig. 8 illustrates the device layout of the interleaver. Grating couplers for TE polarization are employed to couple light with single-mode fibers. Since there is a high reflection power from the grating coupler to the input fiber, it is difficult to measure the reflection spectrum of the interleaver using an optical circulator. We thus inserted a directional coupler before the input port of the interfering loop, and then the reflection spectrum can be measured at port R. The inset of Fig. 8 is a zoom-in view of the interfering loop with three microheaters. The microheater on the waveguide with a length of l_3 is used for wavelength tuning, and the microheaters on the waveguides connecting the directional coupler and the Sagnac loops are used to compensate the phase

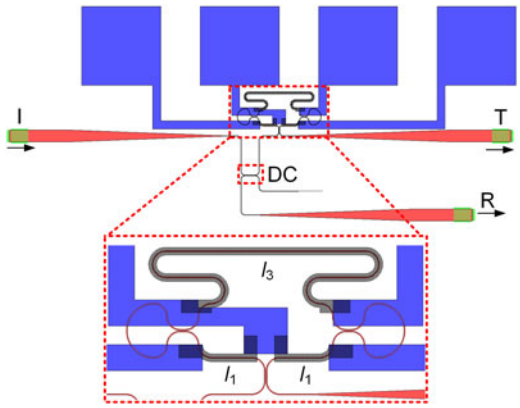

Fig. 8. Device layout of the interleaver. The zoom-in view shows the interfering loop with three microheaters. DC: directional coupler.

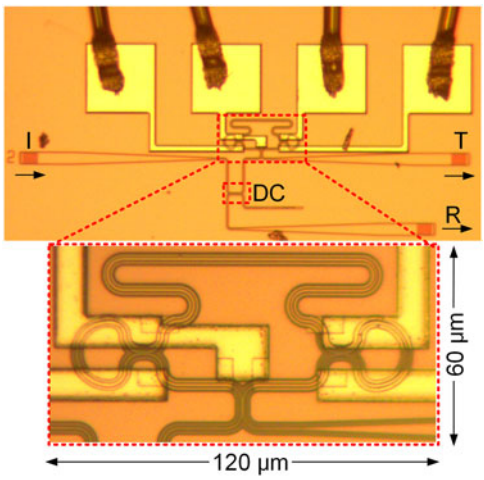

Fig. 9. Micrograph of the fabricated interleaver after wire-bonding.

difference between the two waveguides arising from fabrication errors.

The designed device was fabricated on a silicon-on-insulator (SOI) platform with a 220-nm-thick top silicon layer and a 3-μm-thick buried oxide layer. The cross-sections of the waveguides are 450 nm $\times$ 220 nm. E-beam lithography (EBL) was used to define the device pattern. The top silicon layer was then etched by an inductively coupled plasma (ICP) etching process. A 1-μm-thick silica layer was deposited over the whole device as upper cladding by plasma enhanced chemical vapor deposition (PECVD). 100-nm-thick Ti microheaters and 1-μm-thick Al pads were fabricated using lift-off processes.

Fig. 9 shows the micrograph of the device after wire bonding. The footprint of the interfering loop is 120 μm $\times$ 60 μm. The cavity length of the proposed interleaver is shorter than the circumference of a ring resonator. However, the footprint of the proposed interleaver is similar to that of a well-designed racetrack ring resonator since there are two Sagnac loops in the interleaver. A MZI structure as in [26] can eliminate the need for an off-chip circulator, at the cost of doubled footprint. The coupling lengths of the directional couplers for t_1 and t_2, and the inserted directional coupler are 4 μm, 2 μm, and

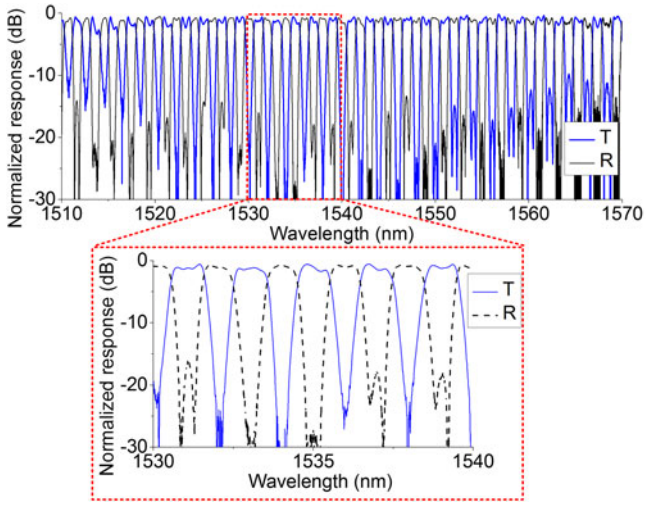

Fig. 10. Measured transmission and reflection spectra in a spectral range of 60 nm. The zoom-in view shows the spectra in a 10-nm spectral range.

13 μm, respectively. The coupling gap is 200 nm for all couplers. Due to fabrication variations, directional couplers with the same coupling length may have different transmission coefficients, thus multiple devices were fabricated.

A continuous-wave tunable laser was used to scan the fabricated device with a step of 5 pm. The fiber-to-fiber coupling loss of the coupling system is $\sim$13 dB. The insertion loss of the interfering loop is $\sim$0.5 dB. The insertion losses in the two arms of the inserted directional coupler are $\sim$5.3 dB and $\sim$1.5 dB, respectively. Therefore, $\sim$5.3 dB and $\sim$6.8 dB additional insertion losses are introduced to the transmission and reflection spectra by the inserted directional coupler, respectively. The additional insertion losses can be avoided by using a MZI structure [26] in practical implementation. Fig. 10 shows the measured transmission and reflection spectra in a 60-nm spectral range. The maximum intensities of the measured transmission and reflection spectra are normalized to 0 dB. The ripples in the stopbands can be attributed to the fabrication-induced phase errors and wavelength dependences of the directional couplers, as discussed in Section III. The inset of Fig. 10 is a zoom-in view of the spectra in a 10-nm spectral range. The FSR is $\sim$1.96 nm, which can be changed by varying l_3 to fit the International Telecommunications Union (ITU) grids. The 20-dB rejection bandwidth is $\sim$0.2 FSR. The in-band ripple is $\sim$1 dB and the 1-dB passband width is $\sim$0.4 FSR. The 3-dB and the 20-dB bandwidths of the passband are $\sim$1.110 nm and $\sim$1.575 nm, respectively, corresponding to a shape factor of 1.42.

The central wavelength shift is demonstrated by tuning the microheater on the waveguide with a length of l_3. Fig. 11(a) shows the measured reflection spectra of the interleaver by applying different heating powers. The central wavelength is red-shifted by 0.575 nm with a heating power of 7.14 mW. The wavelength shifts under various heating powers are shown in Fig. 11(b). It was tuned 2.39 nm with a heating power of 28.57 mW, corresponding to a wavelength-tuning efficiency of $\sim$0.08 nm/mW.

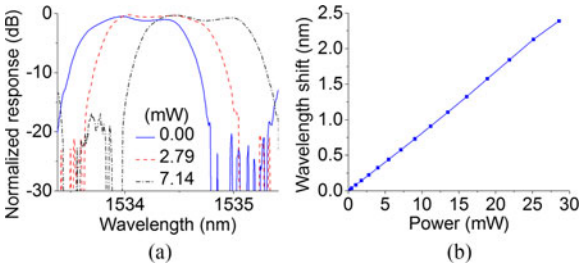

Fig. 11. (a) Wavelength tuning by applying different heating powers. (b) Wavelength shift versus heating power.

V. Conclusion

In this paper, we have presented an extended theoretical analysis and experimental demonstration of a compact silicon photonic interleaver using an interfering loop containing two Sagnac loops. Using the second-order derivative of the intensity transfer function, the transmission coefficients for flattop passbands are calculated. The wavelength dependences of the directional couplers are analyzed to increase the spectral range of the interleaver. The spectral ranges of the measured transmission and reflection spectra of the interleaver are increased to 60 nm with a FSR of ∼1.96 nm. In the wavelength range from 1530 nm to 1540 nm, the 20-dB rejection bandwidth is ∼0.2 FSR and the 1-dB passband width is ∼0.4 FSR. The 3-dB and the 20-dB bandwidths of the passband are ∼1.110 nm and ∼1.575 nm, respectively, corresponding to a shape factor of 1.42. By thermal tuning only one waveguide, the central wavelength can be shifted by more than one FSR with a wavelength-tuning efficiency of ∼0.08 nm/mW.

Acknowledgment

The authors would like to thank the Center for Advanced Electronic Materials and Devices, Shanghai Jiao Tong University, for the support of device fabrication.

References

[1] S. Cao *et al.*, "Interleaver technology: Comparisons and applications requirements," *IEEE/OSA J. Lightw. Technol.*, vol. 22, no. 1, pp. 281–289, Jan. 2004.
[2] T. Mizuno *et al.*, "12.5-GHz spacing compact and low-loss interleave filter using 1.5% Δ silica-based waveguide," *IEEE Photon. Technol. Lett.*, vol. 16, no. 11, pp. 2484–2486, Nov. 2004.
[3] J. F. Song, Q. Fang, S. H. Tao, M. B. Yu, G. Q. Lo, and D. L. Kwong, "Passive ring-assisted Mach–Zehnder interleaver on silicon-on-insulator," *Opt. Express*, vol. 16, no. 12, pp. 8359–8365, Jun. 2008.
[4] L. Zhuang *et al.*, "Nyquist-filtering (de)multiplexer using a ring resonator assisted interferometer circuit," *IEEE/OSA J. Lightw. Technol.*, vol. 34, no. 8, pp. 1732–1738, Apr. 2016.
[5] L. Zhuang *et al.*, "Sub-GHz-resolution C-band Nyquist-filtering interleaver on a high-index-contrast photonic integrated circuit," *Opt. Express*, vol. 24, no. 6, pp. 5715–5727, May 2016.
[6] H. Chien, J. Yu, Z. Jia, Z. Dong, and X. Xiao, "Performance assessment of noise-suppressed Nyquist-WDM for terabit superchannel transmission," *IEEE/OSA J. Lightw. Technol.*, vol. 30, no. 24, pp. 3965–3971, Dec. 2012.
[7] J. Yu and X. Zhou, "Ultra-high-capacity DWDM transmission system for 100G and beyond," *IEEE Commun. Mag.*, vol. 48, no. 3, pp. 56–64, Mar. 2010.
[8] S. Feng, T. Lei, H. Chen, H. Cai, X. Luo, and A. W. Poon, "Silicon photonics: From a microresonator perspective," *Laser Photon. Rev.*, vol. 6, no. 2, pp. 145–177, Apr. 2012.
[9] J. F. Song, Q. Fang, S. H. Tao, M. B. Yu, G. Q. Lo, and D. L. Kwong, "Proposed silicon wire interleaver structure," *Opt. Express*, vol. 16, no. 11, pp. 7849–7859, May 2008.
[10] L. W. Luo *et al.*, "High bandwidth on-chip silicon photonic interleaver," *Opt. Express*, vol. 18, no. 22, pp. 23079–23087, Oct. 2010.
[11] Z. Wang, S. Chang, C. Ni, and Y. Chen, "A high-performance ultracompact optical interleaver based on double-ring assisted Mach–Zehnder interferometer," *IEEE Photon. Technol. Lett.*, vol. 19, no. 14, pp. 1072–1074, Jul. 2007.
[12] J. F. Song *et al.*, "Thermo-optical enhanced silicon wire interleavers," *IEEE Photon. Technol. Lett.*, vol. 20, no. 24, pp. 2165–2167, Dec. 2008.
[13] X. Jiang *et al.*, "Compact silicon photonic interleaver using loop-mirror-based Michelson- Gires-Tournois interferometer," in *Proc. Opt. Fiber Commun. Conf. Exhib*, 2016, Paper Tu2F.5.
[14] B. B. Dingel and M. Izutsu, "Multifunction optical filter with a Michelson-Gires-Tournois interferometer for wavelength-division-multiplexed network system applications," *Opt. Lett.* vol. 23, no. 14, pp. 1099–1101, Jul. 1998.
[15] C. Hsieh *et al.*, "Flat-top interleavers using two Gires-Tournois etalons as phase-dispersive mirrors in a Michelson interferometer," *IEEE Photon. Technol. Lett.*, vol. 15, no. 2, pp. 242–244, Feb. 2003.
[16] X. Jiang, Y. Yang, B. Liu, Y. Zhang, C. Qiu, and Y. Su, "Compact silicon photonic interleaver using an interfering loop containing a Fabry-Perot cavity formed by Sagnac loop mirrors," in *Proc. 42nd Eur. Conf. Exhib. Opt. Commun.*, 2016, pp. 962–964.
[17] S. Orfanidis, *Introduction to Signal Processing*. Englewood Cliffs, NJ, USA: Prentice-Hall, 1996.
[18] C. Madsen and J. Zhao, *Optical Filter Design and Analysis: A Signal Processing Approach*. New York, NY, USA: Wiley, 1999, pp. 305–353.
[19] A. Melloni and M. Martinelli, "Synthesis of direct-coupled-resonators bandpass filters for WDM systems," *IEEE/OSA J. Lightw. Technol.*, vol. 20, no. 2, pp. 296–303, Feb. 2002.
[20] S. Kok, Y. Zhang, C. Wen, and Y. Soh, "Design of all-fiber optical interleavers with a given specification on passband ripples," *Opt. Commun.*, vol. 226, no. 1, pp. 241–348, Sep. 2003.
[21] H. Yamada, T. Chu, S. Ishida, and Y. Arakawa, "Optical directional coupler based on Si-wire waveguide," *IEEE Photon. Technol. Lett.*, vol. 17, no. 3, pp. 585–587, Feb. 2005.
[22] P. P. Absil *et al.*, "Very high order integrated optical filters," in *Proc. Opt. Fiber Commun. Conf. Exhib.*, 2004, Paper TuL3.
[23] K. Zhu, H. Ou, H. Fu, E. Remb, and S. He, "A simple and tunable single-bandpass microwave photonic filter of adjustable shape," *IEEE Photon. Technol. Lett.*, vol. 20, no. 23, pp. 1917–1919, Dec. 2008.
[24] O. Schwelb, "Transmission, group delay, and dispersion in single-ring optical resonators and add/drop filters—A tutorial overview," *IEEE/OSA J. Lightw. Technol.*, vol. 22, no. 5, pp. 1380–1394, May 2004.
[25] J. F. Song, Q. Fang, S. H. Tao, M. B. Yu, G. Q. Lo, and D. L. Kwong, "Silicon nitride-based compact double-ring resonator comb filter with flat-top response," *IEEE Photon. Technol. Lett.*, vol. 20, no. 24, pp. 2156–2158, Dec. 2008.
[26] J. Wang and L. R. Chen, "Low crosstalk Bragg grating/Mach-Zehnder interferometer optical add-drop multiplexer in silicon photonic," *Opt. Express*, vol. 23, no. 20, pp. 26450–26459, Oct. 2015.

Xinhong Jiang received the B.S. and M.S. degrees from Anhui University, Hefei, China, in 2009 and 2012, respectively. He is currently working toward the Ph.D. degree at Shanghai Jiao Tong University, Shanghai, China.

His current research interests include silicon photonics and tunable optical filters.

Yuxing Yang received the B.S. and M.S. degrees from the Chengdu University of Technology, Chengdu, China, and Shanghai University, Shanghai University, in 2010 and 2013, respectively. She is currently working toward the Ph.D. degree at Shanghai Jiao Tong University, Shanghai.

Her current research interests include silicon photonics and nonlinear optics.

Hongxia Zhang received the B.S. from Shandong University, Jinan, China, in 2016. She is currently working toward the M.S. degree at Shanghai Jiao Tong University, Shanghai, China.

Her current research interests include silicon photonics and optical switches.

Jizong Peng received the B.S. degree in electronic engineering from Shanghai Jiao Tong University, Shanghai, China, in 2014, and the Dipl.-Ing. degree from Ecole Centrale de Marseille, Marseille, France, in 2015. He is currently working toward the M.S. degree at Shanghai Jiao Tong University.

His current research interests include optical OFDM, and advanced modulation and detection schemes.

Yong Zhang received the B.S. degree from Northwestern Polytechnical University, Xi'an, China, in 2010, and the Ph.D. degree from Huazhong University of Science and Technology, Wuhan, China, in 2015.

In July 2015, he joined Shanghai Jiao Tong University, Shanghai, China, as a Research Faculty Member. He has published more than 18 journal and conference papers, such as *Optics Letters*, *Optics Express*, and CLEO conference. His research interests include silicon photonics devices and circuit, microcavity devices, E-beam lithography, and ICP etching process.

Ciyuan Qiu received the B.S. and M.S. degrees from Tsinghua University, Beijing, China, in 2005 and 2007, respectively, and the Ph.D. degree from Rice University, Houston, TX, USA, in 2013.

He then worked as Postdoc at Rice University until June 2014. He is currently an Assistant Professor at Shanghai Jiao Tong University, Shanghai, China. He has been the author or coauthor of more than 20 journal articles and conference papers, such as *Nano Letters*, *Scientific Reports*, *Optics Letters*, and *Optics Express*. His current research interests include silicon photonics devices and circuits, graphene optics, and plasmonics.

Yikai Su (S'97–M'01–SM'07) received the B.S. degree from the Hefei University of Technology, Hefei, China, in 1991, the M.S. degree from the Beijing University of Aeronautics and Astronautics, China, in 1994, and the Ph.D. degree in EE from Northwestern University, Evanston, IL, USA, in 2001.

He worked at Crawford Hill Laboratory of Bell Laboratories before he joined the Shanghai Jiao Tong University, Shanghai, China, as a Full Professor in 2004. He has more than 300 publications in international journals and conferences, with more than 2100 citations (Scopus search). He holds 6 U.S. patents and ∼50 Chinese patents. His research interests include silicon photonic devices for information transmission and switching. He served as an advisory board member of Advanced Optical Materials and Advanced Materials Technologies (2015-), an Associate Editor of *APL Photonics* (2016–2018) and *Photonics Research* (2013–2016), a Topical Editor *of Optics Letters* (2008–2014), a Guest Editor of IEEE JOURNAL OF SELECTED TOPICS IN QUANTUM ELECTRONICS (2008/2011), and a Feature Editor of *Applied Optics* (2008). He is the Chair of IEEE Photonics Society Shanghai chapter, a general Co-Chair of ACP 2012, a TPC Co-Chair of ACP 2011 and APCC 2009. He also served as a TPC member of a large number of international conferences including CLEO (2016-), ECOC (2013–2016), OFC (2011–2013), OECC 2008, CLEO-PR 2007, and LEOS (2005–2007). He is a member of OSA.